DOI: 10.1002/cphc.200600604

A Conformational Analysis Method for Understanding the Energy Landscapes of Clusters

Longjiu Cheng,[b] Wensheng Cai,[a, b] and Xueguang Shao*[a, b]

A newly developed unbiased structural optimization method, named dynamic lattice searching (DLS), is proposed as an approach for conformational analysis of atomic/molecular clusters and used in understanding the energy landscape of large clusters. The structures of clusters are described in terms of the number of basic tetrahedron (BT) units they contain. We found that the hit numbers of different structural motifs in DLS runs is proportional to the number of BTs. A parameter T_{max} is defined to limit the maximal number of atoms moved in a structural transition. Results show that T_{max} is a key parameter for modulating the efficiency of the DLS method and has a great influence on the hit number of different motifs in DLS runs. Finally, the effect of potential range on the conformational distribution of the $(Morse)_{98}$ cluster is also discussed with different potential-range parameters.

1. Introduction

Chemistry is based on reactions. The understanding of a reaction is based on the knowledge of the dominant interactions that determine its energy landscape. Therefore, in recent years, energy-landscape theory has emerged as a unifying language for experimentalists and theorists to describe very different reactions, for example, structure formation and dynamics in protein folding, the complex behavior of glasses, and the structure and dynamics of atomic/molecular clusters.[1–6]

The energy landscape describes how the energy of a system changes with geometry. At a minimum, a small displacement in any direction increases the potential energy, just as in a basin surrounded by mountains. For complex systems, the number of local minima on the potential energy surface (PES) is extremely large and the dimension is generally high. As a result, it is almost impossible to directly describe the energy landscape. A number of methods describe the energy landscape indirectly. The energy landscape can be conceptualized as a low-dimensional free-energy surface, with two axes depicting the energy–entropy balance associated with competing physical processes and a ruggedness denoting the presence of frustration that leads to specific kinetic behavior.[3] "Disconnectivity graphs" were proposed to visualize the PES more quantitatively,[7] and a method for describing the PES of atomic clusters by using the disconnectivity graph was developed.[8] On the other hand, the term "funnel" was introduced in describing the situation of protein folding[9,10] and was used to describe the PES of cluster systems.[2,8,11–15] An inherent structure network (ISN) was also employed to represent the topology of energy landscapes, with which local minima and transition states can be represented by nodes and edges.[16] Furthermore, Monte Carlo (MC) simulation[17] and molecular dynamics (MD) simulation[18] were also used for understanding energy landscapes by viewing the residence time in various funnels and translations between funnels.

To understand the PES of a cluster system, an efficient optimization method is necessary, because in some respect the PES consists of local minima. Geometric optimization finds local minima (including the global minimum) on the PES. A good optimization method is the prerequisite for description of the energy landscape. Although the above-mentioned methods can be used successfully to describe the energy landscape of many systems, for more complex systems, more efficient optimization methods are still needed due to the exponential growth of the search space with increasing system size.

There are two kinds of methods for cluster optimization. One consists of modeling methods with lattice searching.[19–21] In such methods, a large and complete lattice with a special motif is built in advance. Then cluster optimization with lattice searching means simply determining which lattice sites should be occupied. In this way, a problem with continuous search space is simplified to a combinatorial optimization problem. Therefore, such methods can be very fast, but the disadvantage is that motifs not contained in the lattice cannot be found and some motifs are difficult to model. The other comprises stochastic global optimization methods, for example, genetic

[a] *W. Cai, Prof. Dr. X. Shao*
Department of Chemistry, Nankai University
Tianjin, 300071 (P. R. China)
Fax: (+86) 22-23502458
E-mail: xshao@nankai.edu.cn
[b] *L. Cheng, W. Cai, Prof. Dr. X. Shao*
Department of Chemistry
University of Science and Technology of China
Hefei, Anhui, 230026 (P. R. China)

algorithms,[22–24] the basin-hopping method,[25–27] conformational space annealing,[28] hierarchical greedy algorithm (HGA),[29] fast annealing evolutionary algorithm (FAEA),[30] random tunneling algorithm (RTA),[31] and adaptive immune optimization method (AIOA).[32,33] Due to the continuity of the search space, in most of these methods, local minimization is adopted to turn the problem into a discrete one. In most of the stochastic optimization methods, the search for new solutions is based on perturbations, and local minimization is necessary after each perturbation. For large clusters, the number of perturbations to find the global minimum is generally very large, and local optimization is always time-consuming due to the complexity of the problem and the large number of parameters to be optimized. Furthermore, due to the characteristic of the energy landscape, going uphill is very difficult when the structure has fallen into a wide funnel. Therefore, stochastic optimization methods are generally not sufficient for large clusters or for clusters with very rough energy landscapes, for example, the $(C_{60})_N$ molecular clusters[34–36] or the Morse clusters[12,37] with a short potential range.[38]

To combine the advantages of the two kinds of method, that is, fast and stochastic, the dynamic lattice searching (DLS) method was proposed.[39,40] In DLS, a lattice-searching approach is adopted to explore new solutions around a locally minimized starting structure instead of perturbations. Application of the DLS method in the optimization of Lennard–Jones (LJ) clusters and $(C_{60})_N$ clusters showed that it is very efficient compared to methods based on stochastic perturbation. Starting from a randomly generated structure, a metastable local minimum (which in some sense corresponds to the lowest local minimum in a "basin" or "funnel" in the basin-hopping method) or the global minimum on the PES can be located after only a few leaps. Therefore, DLS can be used as a tool for conformational analysis of cluster systems.

2. Theory and Methods

2.1. Dynamic Lattice Searching

DLS starts from a randomly generated and locally minimized structure of a cluster. Then all possible vacant sites around the structure can be found. The surface atoms with higher energy (active atoms) in the structure and the vacant sites are termed dynamic lattice. Finally, by searching the lattice with a simple greedy method (SGM), local minima with lower energy can be found. By repeating the lattice-construction and lattice-searching procedures until no minimum with lower energy can be found, the global minimum can be found. Therefore, a DLS run includes generation of the starting structure and repeated lattice construction and lattice searching. In generating the starting structure and lattice searching, local minimization is used to minimize the structure to a local minimum.

In the previous version of DLS,[39] the possible vacant sites around a cluster are located by testing from starting points in various directions with a local minimization approach. But in this study, the starting points for the potential vacant sites are modeled by a geometric method. In this method, all the triangular planes on the surface of a cluster structure are found first; then, for each triangular plane, the two points that form a regular tetrahedron on both sides of the triangular plane are located. If no atom is near the point (less than the unit length of the regular tetrahedron), it is adopted as a starting point for a vacant site, and after local minimization to the single site (supposing an atom is in the site), the new position is taken as a dynamic lattice site. Compared with the previous version, the geometric method is much faster, and it promises to find all possible vacant sites around the cluster. Note that the geometric method is related to the packing style, so for other cases, for example, water clusters or carbon clusters, modifications are needed. Because clusters may be distorted a little after adding or deleting atoms, the dynamic lattice sites are not exact, but they are accurate enough for the lattice searching procedure. Furthermore, because the coordination number of the atoms on the {111} face is 9, only the sites with coordination number less than 10 are taken as dynamic lattice sites in the lattice searching procedure. On the other hand, active atoms are defined as those atoms with higher energy in the previous version of DLS, and a parameter N_{mov} is used to control the number of movable atoms. However, in this work, all the surface atoms (generally with higher energy compared with inner atoms) with coordination number of 9 or less are taken as active atoms (N_{mov}), but the number of moved atoms can be controlled with a parameter T_{max} defined below.

Lattice searching is a key step of DLS which determines the overall performance. Suppose the lattice size is N_L and the number of active atoms is N_{mov}, then the lattice search must occupy N_{mov} atoms in the N_L lattice sites with searching space $C_{N_L}^{N_{mov}}$. For a large cluster, the search space is not small, so an SGM is adopted to search the lattice. First, calculate the total energy of the atoms except for the lattice sites E_C, the energy between each lattice site and the remaining cluster $E_{DLC}(i)$ ($i=1,2,\ldots,N_L$), and the energy of each pair of lattice sites $E_{DL}(i,j)$ ($i,j=1,2,\ldots,N_L$).[39] Then a single SGM procedure can be summarized as follows:

1. Randomly select N_{mov} sites from the lattice to generate a starting solution S_0 and calculate its energy with the established E_C, $E_{DLC}(i)$, and $E_{DL}(i,j)$. Then calculate the energy of each site (occupied or not) in the lattice. For site i, the energy is $E_{DLC}(i)+\sum E_{DL}(i,j)$, where site j is an occupied site.
2. With the current solution S_k ($k=0,1,2,\ldots$), move the atom in the occupied site with highest energy to the vacant site with lowest energy to form S_k', and update the energy of S_k' by subtracting the energy contribution of the original site and adding the energy contribution of the new site.
3. If $E(S_k') < E(S_k)$, take S_k' as the starting solution of the next generation (S_{k+1}) and return to step 2. Otherwise, terminate the iteration with the current solution S_k as the best solution of this SGM search.

The above SGM procedure is very fast. For example, for LJ_{98} the cost of one SGM is only about 1/500 of one local minimization. By running the SGM procedure a reasonable number of times (e.g. 500), various solutions with lower energy may be lo-

cated. Because the lower energy structure found by SGM may slightly change after local minimization, instead of the best one, several (e.g. 10) located solutions with lowest energy will be minimized. If the best located minimum is lower in energy than the current starting structure, it will be accepted as the starting structure of the next repetition, and the lattice-construction and lattice-searching procedures are repeated. Otherwise, DLS will be terminated with the current starting structure as a result.

For a better understanding of the DLS procedure, an illustration for the optimization of the LJ cluster with size $N=98$ (LJ_{98}) is given in Figure 1. Figure 1a shows the case of finding the tetrahedral global minimum, and Figure 1b that of finding the best icosahedral minimum. The structural transition approach is also presented in this figure to show the movements of the atoms in the transition from one structure to another. The number over the arrow is the number of atoms moved from the white sites to the black sites in each transition. It can be seen that, starting from a randomly generated minimum (seed), the metastable minimum structure neighboring the starting seed can be located after several leaps. Of course, DLS may fall into other metastable structures because the seeds are generated randomly. Moreover, the randomly generated seeds should have a higher chance of being contained in a wider funnel on the energy landscape, so the metastable local minima in a wider funnel will have higher chance of being located by DLS.

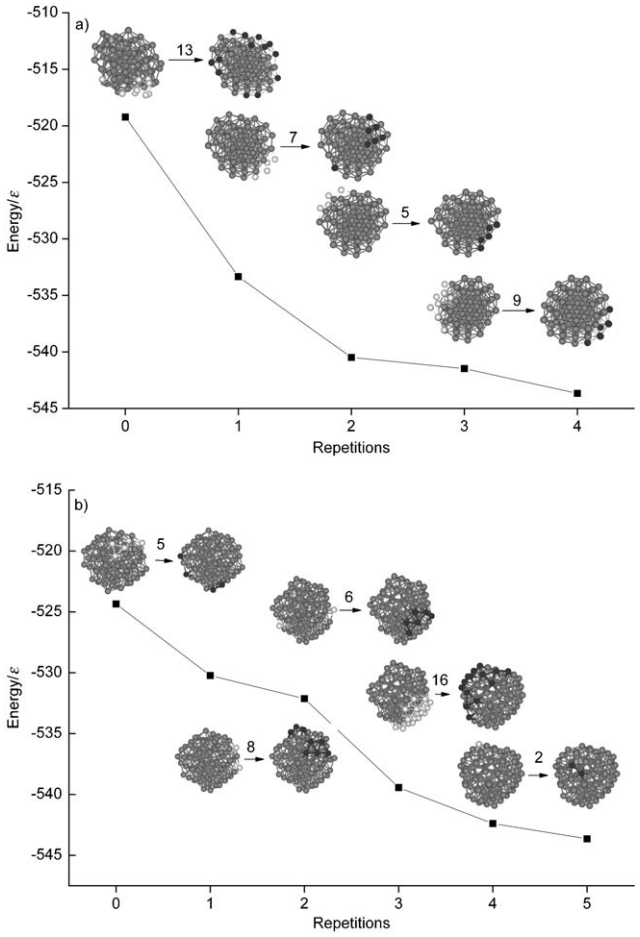

Figure 1. Illustration of a DLS run for LJ_{98}. The *y* axis is potential energy of the minima (ε is pair well depth). DLS starts from a randomly generated minimum whose structure is labeled repetition 0. Then by lattice construction and lattice searching a new lower energy minima is located (repetition 1). The global minimum can be found by repeating lattice construction and lattice searching until no lower energy minima can be found. In the selected cases, starting from random minimum, a) the tetrahedral global minimum of LJ_{98} was found in four repetitions, and b) an icosahedral minimum was found in five repetitions.

For a better understanding of the lattice construction and lattice-searching approach, the last transition (from repetition 3 to repetition 4) in Figure 1a is illustrated in Figure 2. The putative global minimum structure of LJ_{98} is a tetrahedron (Figure 2d), first given by Leary and Doye,[41] which is known as a

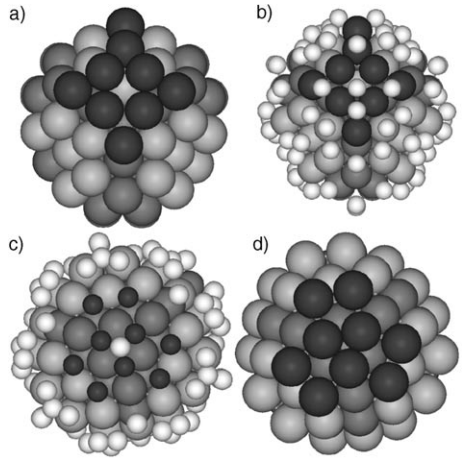

Figure 2. Illustration of a dynamic lattice-searching step for LJ_{98}. a) A local minimum with nine atoms (black balls) that differ in position from the global minimum. b) The modeled dynamic lattice sites (small white balls). c) Back view of (b) in which the small black balls represent the correct locations for the nine atoms in (a). d) Structure of the global minimum.

case that is very difficult to locate with many unbiased global optimization methods.[27,28,33] Figure 2a is a metastable structure (S_0) of LJ_{98} with nine atom locations (black balls) different from the global minimum. Then all possible sites outside the surface of S_0 can be modeled (small white balls in Figure 2b), which denote the dynamic lattice. Figure 2c is a back view of Figure 2b in which the small black balls are in the correct positions for the nine atoms. By searching the lattice with an SGM, the structure can very easily jump to the global minimum from S_0 without any uphill and downhill step. The transition in Figure 2 seems very simple, but in fact it is very difficult for perturbation-based methods; for example, in ref. [42], the transition usually cannot take place after 500 perturbations.

Similar strategies for moving highest energy surface atoms into lowest energy vacancies were adopted in other methods. For example, Hartke[22] developed a method for searching lower energy structures by moving the single worst atom into the best vacant site, and Takeuchi[43] recently developed a very efficient method for global optimization of LJ clusters, in which a surface operator S_m and an interior operator I_m were

developed to move the high-energy atoms. However, the movement operation is very different; for example, in Hartke's method, a single atom was selected, and in Takeuchi's method, a combination of several atoms was used. So, the number of moved atoms must be very small in the latter method due to the large number of possible combinations. In the DLS method, the number of moved atoms can be very large, as shown in Figure 1. In the cases with smooth energy landscapes, for example, icosahedral motifs of LJ clusters, a small number of moveable atoms can gain sufficient efficiency, but for other cases, for example, tetrahedral motifs of LJ clusters or $(C60)_N$ clusters, generally larger numbers of moveable atoms are required to guarantee optimizability.

Evidently, each local minimum located by DLS can be taken as a point on the PES, and the local minima, including the global minimum, found in a large number of runs, can be used to describe the PES of a cluster system. When a new local minimum is found in a lattice search, the current structure jumps to a new position. In some respects, this is like hopping on the PES. In this way, starting from random positions on the PES, various metastable local minima, including the globally most stable minimum, can be visited by hopping. Therefore, a conformational analysis can be carried out by counting the hit numbers of various local minima in a large number of DLS runs. Due to the characteristic of the PES and the statistical property, the local minima in a wide funnel should be visited more frequently than those in a narrow one, because the DLS starts from randomly generated structures. Therefore, an understanding of the energy landscape can be obtained by such conformational analysis approach. Due to the efficiency of the DLS, clusters of comparatively large size can be studied.

On the other hand, in some respects, DLS is similar to the annealing procedure because it finds structures with lower energy by moving the outer atoms. The difference is that only downhill steps are accepted in DLS. In DLS, instead of only one atom, a number of atoms may change their location compared to the starting structure. This is an important characteristic that makes the structural transition in the optimization of DLS easier. In this study, a parameter T_{max} was defined to limit the maximal number of atoms whose location changes in the lattice-searching procedure. With this parameter, the number of moved atoms in a structural transition is limited, and thus T_{max} may affect the search capability of the lattice searching procedure. With this limitation, the relationship of conformational distribution with T_{max} is discussed in Section 3.3. Note that T_{max} is defined just for discussion; in other calculations, the maximal number of moved atoms is not limited, or is only limited by N_{mov}, which is a much larger number than T_{max}.

2.2. Conformational Sequences and Basic Tetrahedra (BT)

Structures of clusters can be sorted by their symmetry and point group. However, in this study, for more convenient conformational analysis, conformations of clusters are sorted by their packings: face-centered cubic (F), F plus a small antilayer (F+), close packing (cp), icosahedral (I), I plus antilayers (I+), face-sharing I (FI), decahedral (D), D plus antilayers (D+), and tetrahedral (T). All these packings are ordered structures with maximal coordination numbers of not more than 12. There are also some low-symmetry packings with maximal coordination number larger than 12, which are called "amorphous" or disordered packings.[38]

Furthermore, the ordered packings can be considered as packed by basic tetrahedra (BT), where the BT can be distorted or incomplete.[40] Figure 3 shows a BT structure and various BTs in the 38-atom fcc (F), 55-atom Mackay icosahedron (I), 75-atom Marks decahedron (D), and 98-atom Leary tetrahedron

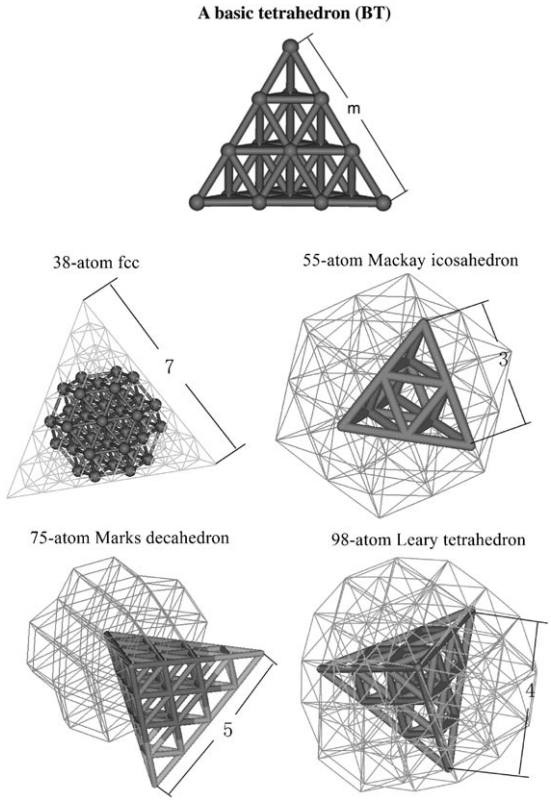

Figure 3. Definition of the basic tetrahedron (BT) in various packings: 38-atom fcc, 55-atom Mackay icosahedron, 75-atom Marks decahedron, and 98-atom Leary tetrahedron. The number is the size of BT (number of atoms in an edge).

(T). As shown in the figure, no BT unit can be found in the structure of the 38-atom fcc, but it can be considered to be contained in a BT unit with 7 atoms in the edge. Also, there is no BT unit in the structure of the 75-atom Marks decahedron, but it can be divided into five parts, each of which can be considered to be contained in a BT unit with a 5-atom edge. For the 55-atom Mackay icosahedron and 98-atom Leary tetrahedron, a complete BT unit with 3- or 4-atom edge can be found in the structure, and the remaining atoms can also be considered to be contained in edge- or face-sharing BT units with the same size. Therefore, the four clusters shown in Figure 3 can be designated 7F, 3I, 5D, and 4T, respectively. If m is the number of atoms in an edge of BT, a sequence with variable m

can be defined, for example, *m*I, *m*I+, *m*FI, *m*F, *m*F+, *m*D, *m*D+, *m*T.

In this way, the BT can be taken as the basic unit of a cluster structure and the number of BT contained in a structure can be easily calculated. For example, as shown in Figure 3, 98-atom 4T is packed by 17 BT, that is, there is one complete BT in the core and four BT which share the four faces of the core BT. For each of the four BT, except for those face-sharing with the core BT, there are another three face-sharing BT. So, the total number of BT contained in the structure is $1+1\times4+4\times3=17$. Similarly, the number of BT of the 38-atom 7F is only 1, 55-atom 3I is packed by 20 slightly distorted edge-sharing BT, and 75-atom 5D is packed by 5 edge-sharing BT. In Section 3.2, the relationship between conformational distribution and the number of BT contained in the structure is discussed.

3. Results and Discussion

3.1. Conformational Analysis for Understanding Energy Landscapes

With disconnectivity graphs, Doye et al.[8,44] successfully studied the energy landscape of small LJ clusters with cluster size $N=$ 13, 19, 31, 38, and 75. In this study, energy landscapes of LJ clusters of larger size are studied. Figure 4 shows the conformational distribution of some selected LJ clusters: LJ_{38} (Figure 4a), LJ_{98} (Figure 4b), LJ_{200} (Figure 4c), and LJ_{400} (Figure 4d). Figure 4 seems somewhat similar to the mass spectrum in outline, but the abscissa is potential energy and ordinate is hit number of various conformations over 1000 independent DLS runs. Based on the principle of DLS mentioned above, a conformation with larger hit number should correspond to the metastable local minima in a wider funnel, so the height (the hit number) and the position on the abscissa (potential) of these peaks correspond respectively to the width and depth of the funnels on the energy landscape. Therefore, conformational analysis with such figures emphasizes more of the appearance (or shape) characteristic of the energy landscape, especially the width and depth, which show the complexity of the energy landscape, while a disconnectivity graph gives more detailed information on the energy landscape.

From Figure 4, the difference of the energy landscape between differently sized clusters can be investigated. First, from Figure 4a it can be seen that there are many disordered structures for LJ_{38}, because the number of possible ordered structures for small clusters is less than that for large clusters. With increasing cluster size, as shown in Figure 4b–d, the number of metastable local minima with ordered structures located by DLS clearly increases. Examination of the located minima and hit numbers shows that, for all the investigated clusters, the number of located icosahedral packings (I, I+, FI) is small but the hit number is comparatively large. This indicates that the landscape of icosahedral motifs is comparatively smooth, so icosahedral local (or global) minima can be easily converged with DLS even for large cluster size, while for other packings the number of located minima is bigger than that of icosahedral packing. This indicates that, compared with icosahedral packing, the landscape of this packing is more complex or there are more metastable local minima on the PES. Interestingly, however, the proportions between the hit numbers of the different packings (I, D, T) do not change too much with cluster size ($N=$38, 98, 200, and 400), and this indicates that, in this range of cluster size, the proportions between the areas of different packings on the PES are similar to each other.

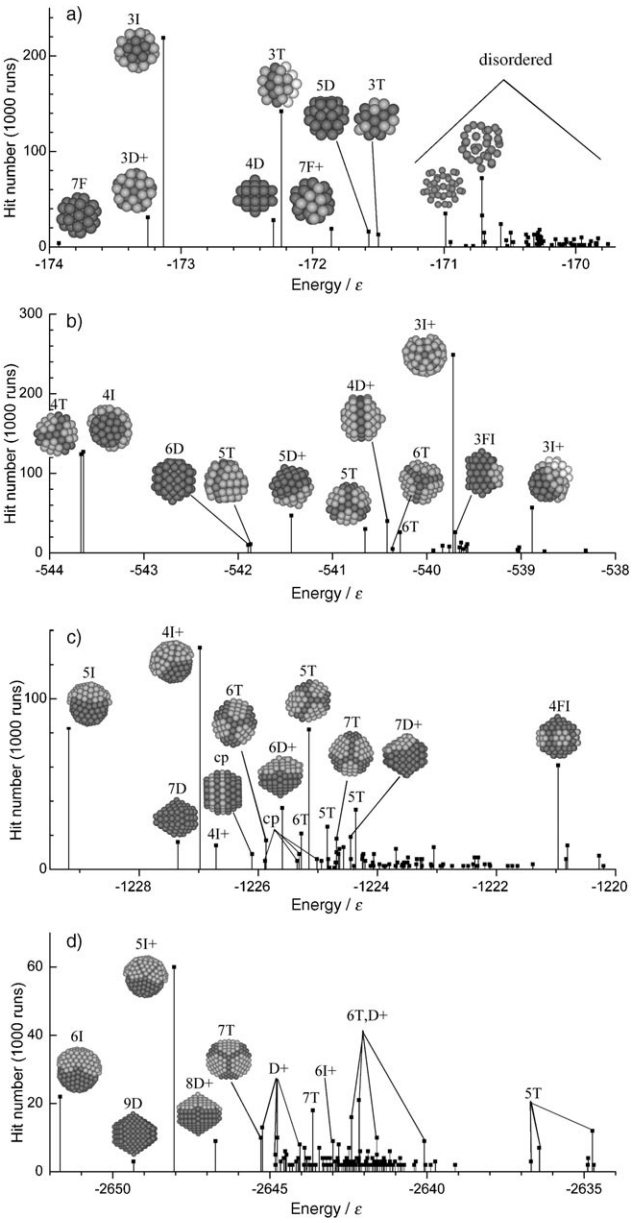

Figure 4. Conformational distribution of LJ clusters obtained by 1000 independent DLS runs for cluster sizes $N=$38 (a), 98 (b), 200 (c), and 400 (d). The *x* axis is the potential energy, and the *y* axis the hit number of each conformation in 1000 DLS runs.

The results can also be compared with those obtained by perturbation-based methods of conformational analysis.[27,42] A figure similar to Figure 4b for conformational analysis of LJ_{98} was also obtained by SGM with energy-based perturbations.[42] By comparing Figure 4b with Figure 3 in ref. [42], it can be found that the the peaks are higher and the number of peaks

is lower in the former. This implies that the small peaks in Figure 3 of ref. [42] merge into the higher peaks in Figure 4b. In fact, all the structures found in Figure 4b and Figure 3 of ref. [42] were compared in detail. Six peaks with similar 4I motif were found that differ only in a few surface atoms, but in Figure 4b there is only one 4I peak. This may be caused by the different strategy for exploring new structures and indicates that DLS is much better converged. DLS finds new structures by moving the atoms on the surface of a cluster, but the SGM in ref. [42] does this by energy-based perturbations. Furthermore, the CPU time for 1000 runs of DLS is only about 10^3 s, while that for the SGM is about 2.2×10^4 s (both with 1.5 GHz Itanium2 processors).

3.2. Relationship of Conformational Distribution with Number of BT

With the definition of the conformational sequences in Section 2.2, it was found that, for different cluster sizes, structures with smaller *m* value correspond to larger hit numbers, and for the same cluster size, the sequence of hit number for various packings is: I+ > I > T > D+ > D > cp, F.[40] This may be the reason why I packings of LJ clusters are easy to locate by stochastic optimization methods, while F and D are difficult.[24,45] For $(C_{60})_N$ molecular clusters, conformational distribution as in Figure 4 can also be obtained by using DLS. Figure 5 shows

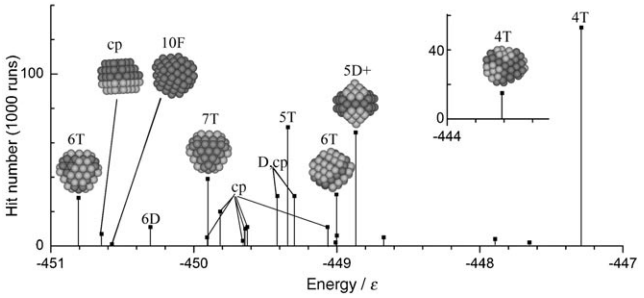

Figure 5. Conformational distribution of $(C_{60})_{98}$ cluster with Girifalco potential obtained by 1000 independent DLS runs.

the conformational distribution of $(C_{60})_{98}$ with Girifalco potential.[34] From both Figure 4 and Figure 5, it can be found that, for all the studied clusters, the packing with a small *m* value corresponds to a large hit number, which completely agrees with the results obtained before.[40]

For further investigation of the relationship between hit number and *m* values, the number of BT and the nearest-neighbor contacts[45] of some favored conformations of LJ_{98} and $(C_{60})_{98}$ are summarized in Table 1. According to the definition above, for I, D, and F motifs, the numbers of BT are 20, 5, and 1 respectively, and for I+, D+, F+, and cp motifs, the antilayers on the {111} faces will increase the number of BT; for example, in the 3I+ motif of the 98 cluster, there are 14 antilayer outer {111} faces of the 55-atom Mackay icosahedral core, so the BT number is 34 (20+14). The number of BT contained in the 4T motif of the 98 cluster was analyzed above. However,

Table 1. Some favored conformations of LJ_{98} and $(C_{60})_{98}$ located by 1000 DLS runs. N_{nn} is the number of nearest-neighbor contacts, N_{Te} the number of BT contained in the conformation, and N_{hit} the hit number of the motif found in 1000 DLS runs.

Clusters	Motifs	Energy/ε	N_{nn}	N_{Te}	N_{hit}
LJ_{98}	4T	−543.665361	432	17	124
	4I	−543.642957	437	20	127
	6D	−541.894959	428	5	10
	5T	−541.869748	429	8	11
	5D+	−541.436260	430	10	47
	6T	−540.362599	427	5	5
	3I+	−539.720452	444	34	249
$(C_{60})_{98}$	6T	−450.805528	427	5	28
	10F	−450.572640	427	1	1
	6D	−450.303293	428	5	11
	7T	−449.902553	426	4	39
	5T	−449.341712	429	8	69
	5D+	−448.868280	427	7	66
	4T	−447.290084	432	17	127

the BT numbers of 5T, 6T, and 7T motifs are smaller because the BT are larger. Motifs with smaller *m* values generally correspond to larger numbers of nearest-neighbor contacts and a larger number of BT, and, as expected, motifs with a larger number of BT are located more frequently for both LJ clusters and C_{60} molecular clusters. There is good correspondence between the number of BT contained in a cluster structure and the conformational distribution.

3.3. Relationship of Conformational Distribution with T_{max}

The calculated results for $(C_{60})_N$ molecular clusters agree with annealing experiments at high temperature,[36,40] but at low temperature, magic numbers observed in the experiments are different from the results of our calculations.[40] Furthermore, calculated results from DLS are different from those of some other theoretical methods with regard to dominant conformations for some LJ clusters. For example, the Leary tetrahedron is very difficult to locate for most stochastic global optimization methods,[27,28,32] while it is a dominant configuration in the results of DLS calculations. Therefore, the conformational distribution obtained by DLS with different T_{max} was investigated.

The conformational distributions with T_{max} for the cases of LJ_{98} and $(C_{60})_{98}$ are given in Figure 6. For each motif, the hit number has an increasing trend with increasing T_{max}, which shows that the efficiency of the DLS method increases with increasing T_{max}, or that the difficulty of structural transition decreases with increasing T_{max}. On the other hand, the increasing trend in hit number also indicates that these motifs are located in deep (stable) funnels of the PES, because they did not jump out into other places with increasing T_{max}. In the case of LJ_{98} (Figure 6a), the hit number of the icosahedral motifs (4I and 3I+) is large even at low T_{max} which implies that the landscape of the motif is wide and smooth, so the structural transition can easily take place even at low T_{max}. However, the hit number for some motifs, for example, 6D, is low over the whole T_{max} range, which implies that the landscape is much

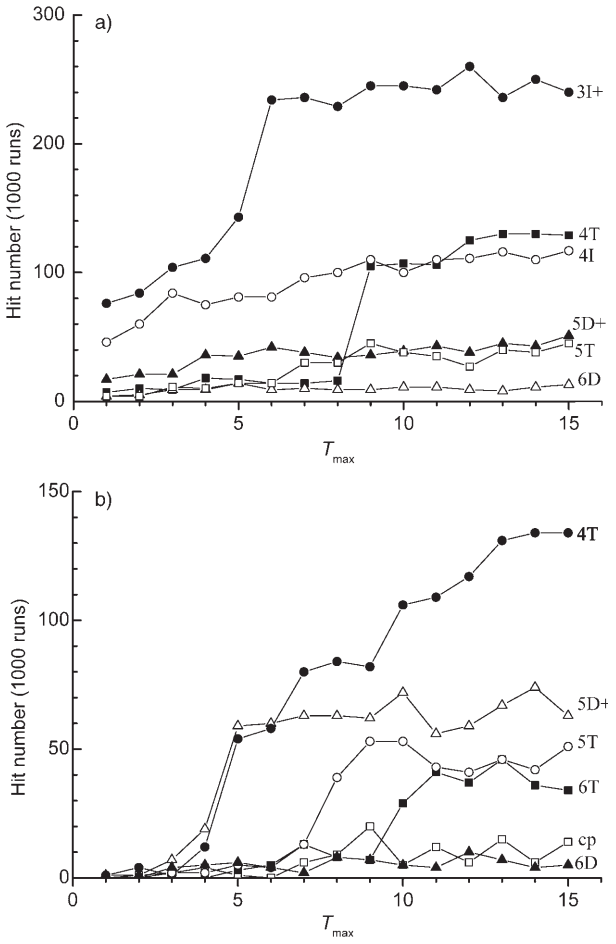

Figure 6. Conformational distribution for some selected motifs as a function of the parameter T_{max} for the cases of LJ_{98} (a) and $(C_{60})_{98}$ with Girifalco potential (b).

narrower. Most interesting is the hit number of the 4T motif, which is very small at small T_{max}, but increases suddenly at $T_{max}=9$. This indicates that the landscape of the motif is wide but very rough, that is, there are many metastable local minima on the PES. On the other hand, the searching performance of the perturbation-based methods should be at the same level as DLS at low T_{max}, and this could explain why the 4T motif is dominant in DLS, while it is a very difficult case for most stochastic optimization methods.

From Figure 6b, it can be seen that, at low T_{max}, the hit number of any motif is small, which means that the energy landscape of $(C_{60})_N$ clusters is much rougher than that of LJ clusters, so structural transitions are difficult at low T_{max}. This also can explain why $(C_{60})_N$ clusters are so difficult to optimize for perturbation-based methods. Furthermore, only at high T_{max} is the 4T conformation dominant, that is, is a large barrier on the PES separates the 4T motif and the other motifs.

3.4. Relationship of Conformational Distribution with Potential Range

The energy landscape is determined by potential. For long-range potential, icosahedral packing is more favored in potential energy, while for short-range potential, decahedral, tetrahedral, and close packing are more favored. Morse clusters[37] can be taken as a test system with the potential function of Equation (1)

$$U_M = \varepsilon \sum_{i<j} e^{\rho_0\left(1-r_{ij}\right)/r_0}\left[e^{\rho_0\left(1-r_{ij}\right)/r_0}-2\right] \quad (1)$$

where the parameter ρ_0 determines the potential range and thus allows it to capture aspects of the interactions for a wide range of systems. For example, the LJ potential has the same curvature at the bottom of the potential well when $\rho_0=6$. Approximating the Girifalco potential for $(C_{60})_N$ clusters gives $\rho_0=13.6$. When ρ_0 is small, the energy landscape is smooth and structural transitions are easy, which makes it not too difficult to locate the metastable local minima and global minimum on the PES. However, for large ρ_0, the extremely short range potential makes the optimization notoriously difficult. For example, Doye et al.[12] reported that, at $\rho_0=14$, even for small clusters with size $N\leq 80$, their method is the first unbiased method that can locate all known global minima. From Figure 6b, it also can be found that, for the Girifalco potential, which is a very short range potential, it is really difficult to locate any local minimum of the investigated motifs at low T_{max} in DLS. This means that the energy landscape is very rough, so the structural transitions are difficult at low T_{max}. But at high T_{max}, DLS achieves very good performance due to its powerful searching capability, achieved by simultaneous movement of several atoms. In our calculations, for each case of Morse clusters with $\rho_0=14$ and cluster size $N\leq 80$, the known global minimum can be located within several minutes on average.

To investigate the effect of potential range, the conformational distribution of some favored motifs of $(Morse)_{98}$ cluster with ρ_0 from 4 to 15 is plotted in Figure 7a. Potential energy of some motifs as a function of ρ_0 is given in Figure 7b. At a very small ρ_0 ($\rho_0=4$), the icosahedral motifs (3I+, 3FI, 4I) are dominant, and the hit numbers increase with increasing ρ_0. However, as seen from Figure 7b, the potential energy of the icosahedral motifs increases rapidly with increasing ρ_0, so the hit numbers of these motifs decrease rapidly to zero when ρ_0 approaches 12. With decreasing hit numbers of the icosahedral motifs, the hit numbers for other motifs, especially that for 4T, increase.

Figure 7 shows that, at large ρ_0, the potential energy of some motifs (4T, 5D+) is much higher than those of the others (Figure 7b), while their hit numbers do not decrease (Figure 7a). Figure 8a plots the strain energy[46] of the selected motifs against ρ_0. The strain energy, calculated according to the method proposed in ref. [46], is a measure of the energetic penalty for deviation of nearest-neighbor contacts from the equilibrium pair distance. Strained motifs may be unstable. For the unstrained motifs (6T, 10F, cp), the strain energy decreases exponentially with increasing ρ_0. For other motifs, the strain energy decreases rapidly with increasing ρ_0 at first but then increases slightly. The decrease is caused by the decrease in compressive strain energy of the atoms in the core, while the

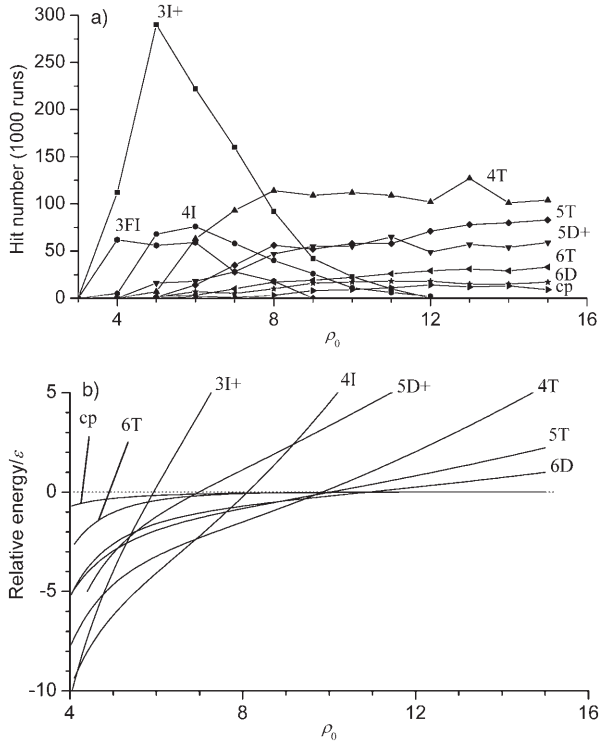

Figure 7. Conformational distribution (a) and potential energy variation (b) of some favored motifs of $(Morse)_{98}$ cluster as a function of ρ_0. On the *y* axis in (b), the energy is relative to that of the fcc (10F) motif to magnify the differences.

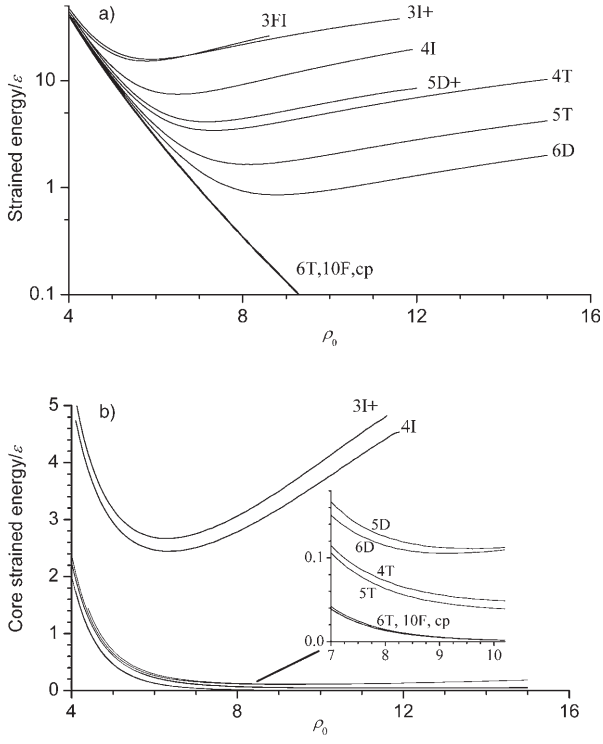

Figure 8. Variation of total strain energy (a) and strain energy of a single core atom (b) of some favored motifs of $(Morse)_{98}$ cluster with ρ_0.

increase is caused by enhancement of the tensile strain energy of the atoms on the surface. Figure 8b plots the strain energy of the single atom in the core of some selected motifs against ρ_0. For the icosahedral motifs, the stain energies of the core atoms of 3I+ and 4I are very high and increase rapidly with increasing ρ_0. This may be the reason why icosahedra are unstable at high ρ_0, while the strain energies of the core atom of other motifs is much lower than that of the icosahedral ones. Therefore, the strain energy of the atom in the core may determine the stability of a cluster motif.

4. Conclusions

A modified version of the DLS method was developed for conformational analysis of cluster systems. With the conformational distribution obtained by DLS, information on the energy landscape is discussed for large LJ clusters, for example, LJ_{400}, and $(C_{60})_N$ molecular clusters. Then, by means of the number of basic tetrahedra (BT) contained in a cluster structure and the parameter T_{max}, which controls the number of atoms moved in the optimization, conformational distributions were investigated. Results indicate that motifs with larger numbers of BT can be located more frequently. It was also shown that T_{max} is a key parameter to modulate the efficiency of the DLS method in finding different cluster motifs. Finally, the conformational distribution of $(Morse)_{98}$ cluster was discussed with different values of ρ_0. It was shown that icosahedra are unstable at high ρ_0 due to the instability of the atom in the core, and the tetrahedron is the dominant motif at high ρ_0.

Acknowledgements

This study is supported by National Natural Scientific Foundation of China (Nos. 20325517 and 20573102) and the Ph.D. Programs Foundation of Ministry of Education of China (No. 20050055001). L.J.C. acknowledges supports from Innovation Foundation for Graduate Students of USTC.

Keywords: cluster compounds · conformation analysis · energy landscapes · global optimization

[1] C. M. Dobson, A. Šali, M. Karplus, *Angew. Chem.* **1998**, *110*, 908 – 935; *Angew. Chem. Int. Ed.* **1998**, *37*, 868 – 893.
[2] D. J. Wales, M. A. Miller, T. R. Walsh, *Nature* **1998**, *394*, 758 – 760.
[3] C. L. Brooks, J. N. Onuchic, D. J. Wales, *Science* **2001**, *293*, 612 – 613.
[4] L. L. Chavez, J. N. Onuchic, C. Clementi, *J. Am. Chem. Soc.* **2004**, *126*, 8426 – 8432.
[5] D. J. Lacks, M. J. Osborne, *Phys. Rev. Lett.* **2004**, *93*, 255 501.
[6] D. J. Wales, *Energy Landscapes*, Cambridge University Press, Cambridge, **2003**.
[7] O. M. Becker, M. Karplus, *J. Chem. Phys.* **1997**, *106*, 1495 – 1517.
[8] J. P. K. Doye, M. A. Miller, D. J. Wales, *J. Chem. Phys.* **1999**, *111*, 8417 – 8428.
[9] P. E. Leopold, M. Montal, J. N. Onuchic, *Proc. Natl. Acad. Sci. USA* **1992**, *89*, 8271.
[10] J. D. Bryngelson, J. N. Onuchic, N. D. Socci, P. G. Wolynes, *Proteins Struct. Funct. Genet.* **1995**, *21*, 167 – 195.
[11] J. P. K. Doye, *Physical Perspectives on the Global Optimization of Atomic Clusters, in Selected Case Studies in Global Optimization* (Ed.: J. D. Pinter), Kluwer, Dordrecht, **2002**, http://arxiv.org/PDF/cond-mat/0007338.

[12] J. P. K. Doye, R. H. Leary, M. Locatelli, F. Schoen, *INFORMS J. Comput.* **2004**, *16*, 371 – 379.
[13] A. M. Sutton, D. Whitley, M. Lunacek, A. Howe, *Proceedings of the 8th Annual Conference on Genetic and Evolutionary Computation*, Seattle, Washington, USA, July 8 – 12, **2006**, pp. 75–82.
[14] M. Locatelli, *Comput. Optim. Appl.* **2005**, *30*, 5 – 22.
[15] S. Goedecker, *J. Chem. Phys.* **2004**, *120*, 9911 – 9917.
[16] J. P. K. Doye, *Phys. Rev. Lett.* **2002**, *88*, 238 701.
[17] W. Polak, A. Patrykiejew, *Phys. Rev. B* **2003**, *67*, 115 402.
[18] W. H. Zhang, L. Liu, J. Zhuang, Y. F. Li, *Phys. Rev. B* **2000**, *62*, 8276 – 8280.
[19] D. Romero, C. Barrón, S. Gómez, *Comput. Phys. Commun.* **1999**, *123*, 87 – 96.
[20] Y. H. Xiang, H. Y. Jiang, W. S. Cai, X. G. Shao, *J. Phys. Chem. A* **2004**, *108*, 3586 – 3592.
[21] Y. H. Xiang, L. J. Cheng, W. S. Cai, X. G. Shao, *J. Phys. Chem. A* **2004**, *108*, 9516 – 9520.
[22] B. Hartke, *J. Comput. Chem.* **1999**, *20*, 1752 – 1759.
[23] R. L. Johnston, *Dalton Trans.* **2003**, 4193 – 4207.
[24] W. Pullan, *J. Comput. Chem.* **2005**, *26*, 899 – 906.
[25] D. J. Wales, J. P. K. Doye, *J. Chem. Phys. A* **1997**, *101*, 5111 – 5116.
[26] D. J. Wales, H. A. Scheraga, *Science* **1999**, *285*, 1368 – 1372.
[27] R. H. Leary, *J. Global Optim.* **2000**, *18*, 367 – 383.
[28] J. Lee, I. H. Lee, J. Lee, *Phys. Rev. Lett.* **2003**, *91*, 080 201.
[29] S. V. Krivov, *Phys. Rev. E* **2002**, *66*, 025 701.
[30] W. S. Cai, X. G. Shao, *J. Comput. Chem.* **2002**, *23*, 427 – 435.
[31] H. Y. Jiang, W. S. Cai, X. G. Shao, *Phys. Chem. Chem. Phys.* **2002**, *4*, 4782 – 4788.
[32] X. G. Shao, L. J. Cheng, W. S. Cai, *J. Chem. Phys.* **2004**, *120*, 11 401 – 11 406.
[33] L. J. Cheng, W. S. Cai, X. G. Shao, *Chem. Phys. Lett.* **2004**, *389*, 309 – 314.
[34] L. A. Girifalco, *J. Phys. Chem.* **1992**, *96*, 858 – 861.
[35] J. M. Pacheco, J. P. Prates-Ramalho, *Phys. Rev. Lett.* **1997**, *79*, 3873 – 3876.
[36] J. P. K. Doye, D. J. Wales, *Phys. Rev. B* **2001**, *64*, 235 409.
[37] P. M. Morse, *Phys. Rev.* **1929**, *34*, 57 – 64.
[38] F. Baletto, R. Ferrando, *Rev. Mod. Phys.* **2005**, *77*, 371 – 423.
[39] X. G. Shao, L. J. Cheng, W. S. Cai, *J. Comput. Chem.* **2004**, *25*, 1693 – 1698.
[40] L. J. Cheng, W. S. Cai, X. G. Shao, *ChemPhysChem* **2005**, *6*, 261 – 266.
[41] R. H. Leary, J. P. K. Doye, *Phys. Rev. E* **1999**, *60*, R6320 – R6322.
[42] L. J. Cheng, W. S. Cai, X. G. Shao, *Chem. Phys. Lett.* **2005**, *404*, 182 – 186.
[43] H. Takeuchi, *J. Chem. Inf. Model.* **2006**, *46*, 2066 – 2070.
[44] J. P. K. Doye, M. A. Miller, D. J. Wales, *J. Chem. Phys.* **1999**, *110*, 6896 – 6906.
[45] The Cambridge Cluster Database, http://www-wales.ch.cam.ac.uk/CCD.html.
[46] J. P. K. Doye, D. J. Wales, *Chem. Phys. Lett.* **1995**, *247*, 339 – 347.

Received: September 27, 2006
Revised: December 25, 2006
Published online on February 7, 2007

